Astronomy & Astrophysics manuscript no. output
August 18, 2026

Interferometric Survey of Stellar Parameters

Constraining the asteroseismic scaling relations with interferometric measurements from the CHARA Array I

M. Vrard[1], D. Mourard[1], O. Creevey[1], S. Deheuvels[2], D.R. Gies[3], N. Ebrahimkutty[1], R.V. Ibañez Bustos[1], J. Jonák[1], H. Nowacki[1], P. Bério[1], J. Dejonghe[1], F. Morand[1], N. Nardetto[1], D. Salabert[1], A. Domiciano de Souza[1], R. Ligi[1], A. Meilland[1], C. Pannetier[4], K. Perraut[5], M. Wittkowski[6], N. Anugu[3], J.D. Monnier[7], S. Kraus[8], M. Gutierrez[7], N. Ibrahim[7], K. Belkacem[9], A. Gallenne[10], K. Kaushik[1], G. Mella[11], T. Morel[12], D.B. Palakkatharappil[13], R.M. Roettenbacher[7], R. Szabó[14,15,16]

[1] Université Côte d'Azur, Observatoire de la Côte d'Azur, CNRS, Laboratoire Lagrange, Bd de l'Observatoire, CS 34229, 06304 Nice cedex 4, France
e-mail: mathieu.vrard@oca.eu
[2] IRAP, Université de Toulouse, CNRS, CNES, UPS, 14 Avenue Edouard Belin, 31400 Toulouse, France
[3] The CHARA Array of Georgia State University, Mount Wilson Observatory, Mount Wilson, CA 91203, USA
[4] LUX, Observatoire de Paris, Universit´e PSL, Sorbonne Université, CNRS, 92190 Meudon, FR
[5] Univ. Grenoble Alpes, CNRS, IPAG, 38000 Grenoble, France
[6] European Southern Observatory, Karl-Schwarzschild-Str. 2, 85748 Garching bei München, Germany
[7] Astronomy Department, University of Michigan, Ann Arbor, MI 48109, USA
[8] Astrophysics Group, Department of Physics & Astronomy, University of Exeter, Stocker Road, Exeter, EX4 4QL, UK
[9] LIRA, Observatoire de Paris, Université PSL, CNRS, Sorbonne Université, Université Paris Cité, 5 place Jules Janssen, 92195 Meudon, France
[10] Instituto de Alta Investigación, Universidad de Tarapacá, Casilla 7D, Arica, Chile
[11] Univ. Grenoble Alpes, CNRS, IRD, INRAE, Météo France, OSUG, 38000 Grenoble, France
[12] Space sciences, Technologies and Astrophysics Research (STAR) Institute, Université de Liège, Quartier Agora, Allée du 6 Août 19c, Bât. B5c, B4000 Liège, Belgium
[13] Université Paris-Saclay, Université Paris Cité, CEA, CNRS, AIM, 91191 Gif-sur-Yvette, France
[14] Konkoly Observatory, HUN-REN Research Centre for Astronomy and Earth Sciences, MTA Centre of Excellence, Budapest, Konkoly Thege Miklós út 15-17, H-1121, Hungary
[15] MTA–HUN-REN CSFK Lendület "Momentum" Stellar Pulsation Research Group, Budapest, Konkoly Thege Miklós út 15-17, H-1121, Hungary
[16] ELTE Eötvös Loránd University, Institute of Physics, Budapest, Pázmány Péter sétány 1/a, H-1117, Hungary

Preprint online version: August 18, 2026

ABSTRACT

Context. Asteroseismic scaling relations are fundamental for the determination of stellar radii and masses. However, recent studies have shown that those relations tend to break down at large radii when compared to other measurements such as radii using photometric and spectroscopic Gaia data. We need independent measurement methods in order to understand and correct those discrepancies.
Aims. In this study, our objective is to investigate the origin of these discrepancies between different methods of radius determination. For this, we are presenting a comparison between the stellar radius estimated with asteroseismology and those measured using interferometry for 19 stars: 8 main-sequence stars and 11 red giants.
Methods. We use the new SPICA (band R) interferometric beam combiner on the CHARA Array, observing simultaneously with two infrared beam combiners: MIRC-X (band H) and MYSTIC (band K). The asteroseismic data consist on *Kepler*, K2 and TESS satellites, as well as ground-based radial velocity observations from SONG for 2 stars.
Results. We present some of the first results using the three instruments simultaneously. The interferometric measurements are consistent between the different bands, and permit the estimation of a stellar radius over a wide spectral domain, allowing a precise comparison with asteroseismic estimations. We found that, to a first approximation, the two approaches give similar results within 2σ uncertainties, even at large radii (R $\simeq 23R_\odot$). Only one star shows discrepancies, likely due to peculiarities of that target. We show no clear temperature or metallicity influence for the correlation between asteroseismic and interferometric radii. We also compare the interferometric radii with different versions of the asteroseismic scaling relations, and find no clear change in the results.
Conclusions. Our large sample of interferometric radius estimations allows us to assess the reliability of classical and modified scaling relations for main-sequence and red giant branch stars, over a wide range of stellar radii (0.8 to $23R_\odot$). The new approach of polychromatic interferometric estimation improves the reliability and precision of the radius estimation. Overall, the various scaling relations are in close correlation with the interferometric observations.

Key words. Stars: oscillations – Stars: evolution – Methods: data analysis – Techniques: interferometry, asteroseismology

1. Introduction

Stellar radius and mass measurements are essential in order to retrieve precise information on stellar populations, exoplanetary systems, and galactic evolution. Asteroseismology has proven to be a powerful method for achieving a precise and accurate stellar radius and mass estimation with little model dependence through the so-called scaling relations (e.g., Kjeldsen & Bedding 1995; Kallinger et al. 2010a). This technique was applied on thousands of solar-like pulsators (e.g., Yu et al. 2018) particularly since the launches of the CoRoT (Baglin et al. 2006), *Kepler* (Borucki et al. 2010) and the Transiting Exoplanet Survey Satellite (TESS) (Ricker et al. 2015) photometric missions. The future space photometric mission PLAnetary Transits and Oscillations of stars (PLATO) (Rauer et al. 2025) will continue to increase the number of stars for which asteroseismic analysis is performed.

The very wide use of seismic scaling relations has motivated extensive efforts to quantify both their precision and their accuracy. While statistical uncertainties of a few percent in radius and around 5-10% in mass, depending if we consider main-sequence or red giant objects, can often be achieved for high-quality data, the assumptions that are made to establish these relations can limit their accuracy. Therefore, a considerable body of work has been dedicated to testing and improving the seismic scaling relations. Corrections to the $\Delta\nu$ scaling based on stellar models have been proposed to account for departures from simple mean-density scaling, particularly along the red giant branch and in core-helium-burning stars (e.g., White et al. 2011b; Miglio et al. 2013; Sharma et al. 2016; Rodrigues et al. 2017). It has been more difficult to test the $\nu_{\rm max}$ relation, whose empirical success is well established, but whose theoretical foundation remains less secure than that of $\Delta\nu$ (e.g., Belkacem et al. 2011; Viani et al. 2017).

Independent validation has also been attempted using a diversity of complementary techniques. The combination of high-precision Gaia parallaxes with bolometric fluxes has enabled large-scale tests of asteroseismic radii across the Hertzsprung–Russell diagram (Huber et al. 2017; Sahlholdt & Silva Aguirre 2018; Zinn et al. 2019). These studies generally find agreement between asteroseismic and astrometric radii at the level of a few percent for main-sequence stars and low-luminosity red giants, but discrepancies were reported for more luminous red giant stars (Zinn et al. 2019, 2023; Pinsonneault et al. 2025). Detached eclipsing binaries containing oscillating red giants provide among the most stringent tests because masses and radii can be measured dynamically with high precision. Early comparisons suggested that the classical scaling relations systematically overestimate red giant masses by up to $\sim 15\%$ and radii by about 5% (Gaulme et al. 2016; Benbakoura et al. 2021). Subsequent investigations demonstrated that applying theoretically motivated corrections to the $\Delta\nu$ scaling relation substantially improves the agreement between seismic and dynamical masses and radii for several benchmark eclipsing binaries (Brogaard et al. 2018), although the full sample of Gaulme et al. (2016) still exhibits residual discrepancies whose origin remains under investigation.

Send offprint requests to: mathieu.vrard@oca.eu

Additional independent tests can be provided by long-baseline optical interferometry, which allows direct measurements of stellar angular diameters, therefore radius, with an estimation of the stellar parallax (Labeyrie 1975; Eisenhauer et al. 2023). The comparison between asteroseismic and interferometric data was already performed previously on a few dozens of targets (Huber et al. 2012; White et al. 2013; Baines et al. 2014; Johnson et al. 2014; Stokholm et al. 2019; Karovicova et al. 2022a,b) which allowed to conclude that the scaling relations were robust for main-sequence and small red giant stars. However, some discrepancies were found for more evolved red giants (Karovicova et al. 2022b) and the limited number of targets did not allow to extend the conclusion towards low-mass main sequence targets and stars above R $> 15R_{\odot}$. Moreover, the increase of precision and accuracy with the publication of the Gaia parallaxes are now bringing new precision on the radius estimation. In this work, we conduct a survey of interferometric observations of asteroseismic targets in order to assess the range of validity of the scaling relations and increase their precision and accuracy. We also test the different versions that were proposed to the asteroseismic scaling relations in order to investigate their proposed improvement in terms of the precision and accuracy compared to the classical scaling relations.

To achieve this objective, we utilize the CHARA (Center for High Angular Resolution Astronomy) interferometer located at Mount Wilson Observatory with the instruments MYSTIC (Michigan Young STar Imager at CHARA; Setterholm et al. 2023), MIRC-X (Michigan InfraRed Combiner-eXeter; Anugu et al. 2020) and SPICA (Stellar Parameters and Images with a Cophased Array; Mourard 2026), operating simultaneously. MIRC-X (resp. MYSTIC) is a 6-telescope beam combiner in H-band (resp. K-Band), while SPICA is a new 6-telescope beam-combiner in R-band. Interferometric data are thus recorded for the first time simultaneously in R, H, and K bands, a unique feature especially for asteroseismic targets.

This work was performed in the context of the Interferometric Survey of Stellar Parameters (ISSP, Mourard 2026), which aims to complete and exploit a large survey of stellar parameters through the use of the CHARA interferometer and particularly its new visible instrument SPICA. This interferometric survey on bright stars in the local environment serves different purposes: star's characterization, exoplanetology, galactic archeology, distance estimation. This paper presents the first results concerning the asteroseismic low-mass star pulsators, for main-sequence stars, subgiants, and red giants. The objective is to combine asteroseismology and interferometry to obtain the most precise stellar parameters for a large sample of targets across the Hertzsprung-Russell diagram, with the ultimate goal of improving the calibration of the asteroseismic scaling relations and refining the models using the highest quality sample.

This paper is organized as follows: Section 2 describes the target selection for the asteroseismic part of the ISSP survey. Section 3 details the interferometric observations and the whole set of interferometric and asteroseismic data. Section 4 shows the interferometric data processing. Section 5 describes the determination of the stellar fundamental parameters with the interferometric and asteroseismic data. Section 6 is devoted to the comparison between the asteroseismic and interferometric radius. Section 7 presents the conclusion and discusses the perspectives.

2. Complete sample selection

For the main-sequence sample, the selection is made from the confirmed CoRoT, *Kepler*, K2 and TESS pulsators based on previous measurements (Carrier et al. 2005b,a; Carrier & Eggenberger 2006; Bedding et al. 2007; Teixeira et al. 2009; Benomar et al. 2009; Kallinger et al. 2010b; Appourchaux et al. 2012; Mathur et al. 2012; Silva Aguirre et al. 2012, 2013; Bazot et al. 2012; Huber et al. 2013; Metcalfe et al. 2014; Liu et al. 2014; Chaplin et al. 2015; Lagarde et al. 2015; Baglin & Michel 2015; Guzik et al. 2016; Lund et al. 2016, 2017; Grundahl et al. 2017; Van Eylen et al. 2018; Huber et al. 2019; Lund et al. 2019; Campante et al. 2019; Chaplin et al. 2020; Nielsen et al. 2020; Malla et al. 2020; Ball et al. 2020; Jiang et al. 2020; Metcalfe et al. 2020; Adassuriya et al. 2021; Chontos et al. 2021; Addison et al. 2021), which gave us 799 stars with asteroseismic parameters and within reach of the SPICA instrument. We added 358 targets that are included in the list of benchmark stars for the PLATO mission (Rauer et al. 2025). These stars correspond to bright targets that will be used to test the PLATO pipelines and models, thus helping to better model PLATO targets (Zwintz et al. 2026). We added the new observations done by the TESS satellite on luminous main-sequence targets (Lund et al. 2025). For the red giant and subgiant asteroseismic sample, the selection was performed in a similar way. We selected targets observed with CoRoT, *Kepler* (Yu et al. 2018), K2 (Pope et al. 2019, Grunblatt et al. 2019) and TESS with deduced asteroseismic global parameters (the large separation $\Delta\nu$ and frequency of maximum oscillation $\nu_{\rm max}$). For the TESS sample, we specifically focused on the sample of luminous stars in the continuous viewing zones observed by Hon et al. (2022).

Following the construction of those lists, the definitive sample was selected with several criteria. The first was observability: the target has to be observable from the northern hemisphere, thus we focus on the stars with a declination $\delta > -30$ deg. The second criterion was based on the magnitude limitation of SPICA in the visible: stars with $m_V > 9$ were therefore excluded from the sample, $m_V > 8$ for red giants and subgiants for which we had a larger sample. The third criterion corresponds to the estimated angular diameter. Using the Surface Brightness-Color Relationship (SBCR), calibrated for main-sequence, subgiant and red giant objects by Salsi et al. (2020, 2021), we can deduce the expected angular diameter by using the magnitudes in different spectral bands ($V-K$). If the expected angular diameter $\theta < 0.2$ mas, then the star was excluded from the sample since the resolution of the SPICA instrument will not be sufficient to resolve the target. With these criteria, we obtain a final sample of 432 main-sequence, 441 red giant and 6 subgiant stars. Among the red giant sample, 211 have TESS asteroseismic data and 230 have *Kepler* and CoRoT data. Among those, we selected 50 main-sequence stars as priority targets to be observed based on the expected precision on the obtained interferometric radius and a good coverage of the HR diagram. Similarly, we selected 60

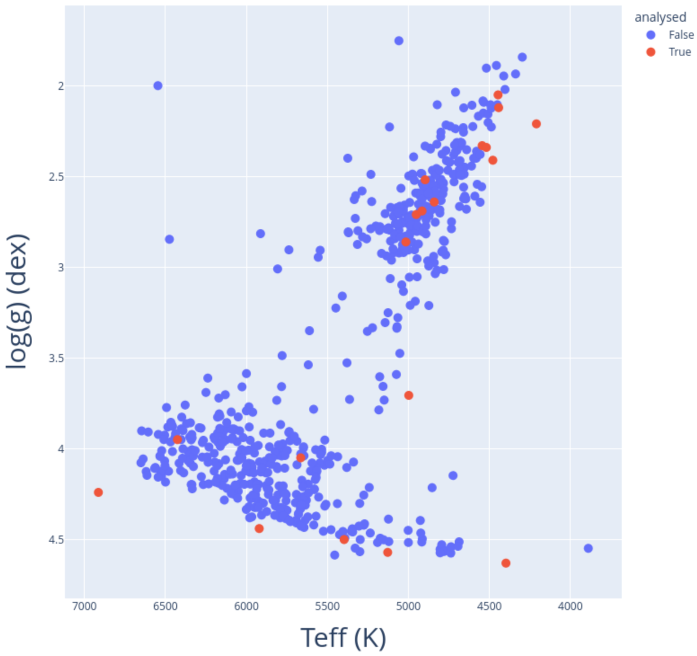

Fig. 1: Kiel diagram for the full sample of main-sequence and red giant stars (in blue). The red dots correspond to the stars that were observed for this work. The $T_{\rm eff}$ and log(g) estimations come from the Gaia/DR3 GSP-Spec module (de Laverny et al. 2026).

stars among the red giant and subgiant sample as priority targets, for covering mass, evolutionary status and metallicity range with the most luminous object in each category.

With this final sample of 879 stars (see Fig. 1), we have a sufficient coverage of solar-like pulsators with asteroseismic data for which we can obtain interferometric observations from SPICA. This initial large sample permits an optimal selection of targets following the organization of the observing nights dedicated to the ISSP survey and the progress of its completion. This first article establish the methods and shows the feasibility of obtaining precise constraints on the asteroseismic scaling laws with the first observations conducted between 2023 and 2025. It will be followed by other publications with the continuation of the observation programs throughout 2026 and 2027 for which we expect a final sample with a sufficient coverage in terms of mass, metallicity and evolutionary state so we can efficiently constrain scaling relations following those characteristics.

3. Presentation of the data

3.1. Interferometric observations and data processing

Interferometric observations were obtained between August 2023 and September 2025 with the SPICA, MIRC-X, and MYSTIC instruments at the CHARA Array. The details of the observations are given in Table 1. We manage to obtain 44 observations of 19 different stars: 8 main sequence stars and 11 red giants. For the calibration of the interferometric transfer function, reference stars are identified using the JSDC (JMMC Stellar Diameters Catalog) (Chelli et al. 2016; Bourges et al. 2017) giving estimation of the equiva-

Table 1: Journal of observations.

Star	Instrument	Date (yyyy.mm.dd)	Calibrators[1]
HD 173667	S	2023-08-09	HD184606, HD196740
	SMM	2024-06-12	HD166230, HD189849
	SMM	2025-04-23	HD143894^{S,Y}, HD168914
	SMM	2025-05-09	HD157198, HD168914, HD189849^{I,Y}
HD 185395	S	2023-08-07	HD177196, HD147394
	MM	2024-05-10	HD144206^{Y}, HD159541, HD177196
	SMM	2024-06-10	HD192514, HD198639
	SMM	2024-06-11	HD144206^{Y,I}, HD159541, HD192514
	SMM	2024-08-19	HD160762^{Y,S}, HD195556^{Y,S}, HD213558^{Y,I}, HD222173^{I}
	SMM	2025-06-14	HD159541^{Y,I}, HD184171, HD192514
HD 161797A	SMM	2024-07-04	HD141003, HD143894^{Y,I}, HD173667, HD196724^{Y}
	SMM	2025-04-23	HD143894^{S,Y}, HD168914
	SMM	2025-06-13	HD143894^{Y}, HD154494, HD166182, HD195810^{I}
	SMM	2025-08-18	HD184606, HD196724
HD 10700	MM	2024-08-18	HD200761^{Y}, HD21790, HD225132
	S*MM	2024-09-14	HD219832^{S,Y}, HD203705^{I}
HD 22049	S*MM	2024-09-13	HD21790
	S&MIRC-X	2025-09-15	HD7804, HD15318, HD21790, HD27861
HD 160269A	SMM	2025-05-10	HD163989, HD182564^{S,I}
HD 201091	SMM	2025-06-14	HD184171^{S,Y}, HD192514, HD207260^{I,Y}
HD 23249	S&MIRC-X	2025-09-15	HD7804, HD15318, HD21790, HD27861
HD 28305	SMM	2023-10-14	HD7964^{S,I}, HD20150, HD26912^{S,Y}, HD31295^{S,I}
HD 6186	S	2023-09-25	HD217891, HD220825, HD20150
	SMM	2024-08-16	HD886, HD16582^{S,Y}
	S*&MIRC-X	2024-11-02	HD21790, HD42690
	S*&MIRC-X	2025-08-17	HD1064^{I}, HD6530^{I}, HD15130^{S}, HD18331
HD 27371	S&MYSTIC	2023-09-26	HD7964, HD14191^{S}, HD21686, HD26912^{S}
	SMM	2023-10-14	HD7964^{S,I}, HD20150, HD26912^{S,Y}, HD31295^{S,I}
	SMM	2023-11-10	HD20150, HD23338^{S,I}, HD87737^{Y}
HD 148387	MM	2024-05-17	HD144206, HD159541, HD177196^{Y}
HD 163588	MM	2024-05-17	HD144206^{Y}, HD159541, HD177196
	S*MM	2025-05-11	HD159541, HD177196^{I,Y}
	S*M*M*	2025-05-12	HD90839^{I}, HD115735, HD177196^{Y}
	S&MIRC-X	2025-06-14	HD159541^{I}, HD184171, HD192514
HD 170693	MM	2024-05-19	HD125162, HD182564
	SMM	2025-06-15	HD182564
HD 176524	SMM	2024-07-07	HD164613^{I,Y}, HD182564, HD213558^{S}, HD222173^{S}
	SMM	2025-06-15	HD182564
HD 180711	MM	2024-08-17	HD214734
HD 181984	MM	2024-08-17	HD214734
HD 28292	MM	2024-09-12	HD20150, HD30210^{I}
HD 31539	SMM	2025-09-14	HD7804^{I,Y}, HD21790, HD27861

Notes. 1: diameters of calibrators are from Bourges et al. (2017)
S: SPICA instrument; MM: MIRC-X and MYSTIC instruments.
* Observation was considered as being not exploitable
S,I,Y: calibrators used only for the respective instruments SPICA (S), MIRC-X (I) and MYSTIC (Y)

lent uniform disk angular diameters in the different spectral bands.

The raw data of the three instruments are first preprocessed by their respective pipelines (Mourard 2026 for SPICA, Anugu et al. 2020 for MIRC-X and MYSTIC), producing uncalibrated oifits files (Duvert et al. 2017) for all science targets and reference stars. The second step of the processing is done by using the same calibration tool for the three instruments. It has been developed initially for SPICA (Mourard 2026) and has been adapted to accept also MIRC-X and MYSTIC data. This tool permits to select calibrators close in time, to flag baselines or spectral channels with poor signal to noise, and generates the calibrated oifits files. These selections are made by inspecting the initial uncalibrated data, then with the estimations of the transfer functions provided by the quality check documents produced by the calibration tool, and finally with the calibrated data themselves. We also checked the closure phases for each observation of each stars and calibrators in order to establish that all those objects does not show sign of binarity or astrometric perturbations. No significant signature of binarity was detected for the MIRC-X, MYSTIC and SPICA observations of both stars and calibrators. The oifitsexplorer[1] software is used for this purpose. All the calibrated data used in this paper

[1] Available at http://www.jmmc.fr/oifitsexplorer

are available through the OiDB database[2] (Haubois et al. 2014).

In addition, the current MIRC-X/MYSTIC pipeline does not account for a miscalibration of wavelength affecting the instrument. As noted by the MIRC-X/MYSTIC Pipeline Manual[3], based on a comparison with results obtained with the VLTI/GRAVITY instrument (GRAVITY Collaboration et al. 2017), we corrected this effect by dividing the measured wavelength by an instrument-dependent constant factor (i.e. $\lambda_{\rm true} = \lambda_{\rm measured}/\kappa$):

$$\begin{aligned} \kappa_{\rm MIRC\text{–}X} &= 1.0054 \pm 0.0006, \\ \kappa_{\rm MIRC\text{–}X} &= 0.999 \pm 0.001 \text{ (year 2025)}, \\ \kappa_{\rm MYSTIC} &= 1.0067 \pm 0.0007, \\ \kappa_{\rm MIRC} &= 1.0014 \pm 0.0006. \end{aligned} \quad (1)$$

3.2. Asteroseismic data description

For the 19 stars that were observed, we took asteroseismic data from various sources (see Table 2 for a list of the data provenance). We extracted the large frequency separation $\Delta\nu$ and frequency of maximum oscillations $\nu_{\rm max}$ from those different references. $\nu_{\rm max}$ is related to the cut-off frequency, therefore to the stellar gravity and $T_{\rm eff}$ (Belkacem et al. 2011), while $\Delta\nu$ scales approximately to the stellar density estimation (Kjeldsen & Bedding 1995). Among the available sources, there is only one star (HD185395) for which 4-year *Kepler* data are present. The asteroseismic analysis of this target was previously done by Guzik et al. (2016) with a precise extraction of the mode frequencies. This star has therefore the most precise and accurate asteroseismic measurements in our sample. Most of the stars in our sample possess TESS asteroseismic data and were already analyzed by Hon et al. (2022) and Lund et al. (2025). The red giants Hon et al. (2022) studied are present in the Continuous Viewing Zones (CVZ) of TESS, therefore having up to 1 year of continuous light-curves. Thus, the extracted global seismic parameters ($\Delta\nu$, $\nu_{\rm max}$) from these light-curves are reliable (Mosser et al. 2019). The main-sequence bright targets of Lund et al. (2025) are more randomly dispersed in the sky and have mostly shorter duration light-curves. However, after 3 years of TESS observations, the length of those light-curves are mostly above 4 months. It is thus likely that the deduced asteroseismic data are of decent quality. A large part of the sample was also observed by K2 (Pope et al. 2019) with 3 months of photometric data. This short duration, and the lower stability of the satellite during the K2 mission, negatively affect the reliability of the asteroseismic parameters (Stello et al. 2017). This will be taken into account during the rest of the study.

For 2 stars, only ground-based observations are available from published data. HD161797 has been extensively observed by the SONG telescopes since 2014 (Grundahl et al. 2017; Gupta et al. 2025), leading to very precise global asteroseismic parameters. In contrast, HD10700 has been observed with ground-based HARPS data only once in 2004 during a 5-night observation session (Teixeira et al. 2009). More recently, Lund et al. (2025) tried to extract the asteroseismic parameters from the TESS satellite data for that star, but without success. We also extracted asteroseismic data from the TESS light-curve for that target but reach the same conclusion. It results in only a faint oscillations signal for ground-based observations that is available for that star. Therefore, this asteroseismic data will be considered with caution in the rest of the article.

Finally we have 2 stars in our observed sample for which we have TESS light-curves, however oscillations were not discovered. HD22049 was analyzed by Lund et al. (2025) but no oscillations were successfully detected, therefore determining the global asteroseismic parameters was not possible. HD201091 was not studied by Lund et al. (2025), but suffers a similar situation. We also extracted the light-curves from TESS for those two targets and reach the same conclusion. We decided to discard those two targets from the observed sample for the rest of the study. A summary of the final asteroseismic data selected for this study is present in Table 2.

[2] OIDB available at http://oidb.jmmc.fr

[3] v0.9.6, May 24 2024

4. Angular diameter and radius estimations

4.1. Angular diameter

The estimation of the angular diameters is performed by a model fitting process using the `oimodeler` code (Meilland et al. 2024). We use the MCMC minimization process of the code to fit over the observations a square root Limb-Darkening (LD) model:

$$\frac{I(\mu)}{I(1)} = 1 - c(1-\mu) - d(1-\sqrt{\mu}), \quad (2)$$

where $I(1)$ is the intensity at the center of the disc, c and d are the limb-darkening coefficients and μ is defined by $\mu = \cos\gamma$, where γ is the angle between the line of sight and the emergent intensity. Ebrahimkutty et al. (2024) performed several investigations on the different limb-darkening models and concluded that the square root LD model is the most reliable, particularly near the first 0 in square visibility. Considering the frequency coverage of the observations and the measurement noise, we decided to fix the coefficients c and d and adjust the diameter only. For each band, the coefficients are taken from Claret & Bloemen (2011), taking into account the star $T_{\rm eff}$, log(g) and metallicity from the same spectroscopic catalogs indicated in Section 4.3. MIRC-X and MYSTIC exhibit sometimes some calibration issues at short baselines. If the star is not resolved sufficiently, this could introduce a bias in the diameter determination. This issue was solved by adding a background to the model and adjusting the relative intensity of this background with respect to the disc. This was only considered for MIRC-X and MYSTIC data since all stars in our observed sample are resolved with SPICA.

As a first step, the analysis is done night by night and instrument by instrument. It permits to assess the reliability of the estimate of the angular diameters and to detect any possible bias or miscalibration issues. Examples of the fits on the different bands are presented in Figure 2 for the star HD201091. The number of flagged bad quality baselines on SPICA data can be important for some observations, therefore the fitting was not possible on these cases, particularly

Table 2: Asteroseismic, spectroscopic and astrometric parameters for the observed stars.

HD number	$\Delta\nu$ (μHz)	$\nu_{\max}$ (μHz)	seismic origin	$T_{\rm eff}$ (K)	[Fe/H]	spectroscopic origin	π (mas)
HD 185395	83.9 ± 0.4	1829 ± 54	*Kepler*[1]	6914 ± 33	-0.03 ± 0.03	Gaia FGK benchmark stars[a]	54.27 ± 0.09
HD 173667	56.2 ± 1.6	1061 ± 28	TESS[2]	6426 ± 20	-0.04 ± 0.02	Gaia FGK benchmark stars[a]	51.67 ± 0.12
HD 161797A	64.2 ± 0.2	1216 ± 11	SONG[3]	5665 ± 16	0.25 ± 0.01	Gaia FGK benchmark stars[a]	119.92 ± 0.15
HD 10700	169.3 ± 0.3	4490 ± 225	HARPS[4]	5397 ± 15	-0.51 ± 0.01	Gaia FGK benchmark stars[a]	273.81 ± 0.17
HD 22049	–	–	–	5128 ± 22	-0.05 ± 0.01	APOGEE[b]	310.58 ± 0.14
HD 160269A	132.9 ± 0.9	3059 ± 177	TESS[2]	5921 ± 33	-0.04 ± 0.03	Gaia FGK benchmark stars[a]	69.28 ± 0.20
HD 201091	–	–	–	4398 ± 34	-0.13 ± 0.03	Gaia FGK benchmark stars[a]	285.99 ± 0.06
HD 23249	41.5 ± 0.8	677.6 ± 8.3	TESS[2]	4998 ± 9	0.07 ± 0.01	APOGEE[b]	110.03 ± 0.19
HD 6186	3.62 ± 0.07	33.31 ± 1.22	K2[6]	4897 ± 13	-0.28 ± 0.01	APOGEE[b]	17.81 ± 0.18
HD 27371	5.72 ± 0.07	62.59 ± 1.74	K2[6]	4952 ± 30	0.10 ± 0.02	PASTEL[c]	21.66 ± 0.18
HD 28305	5.13 ± 0.13	54.46 ± 1.44	K2[6]	4916 ± 17	0.14 ± 0.02	PASTEL[c]	22.37 ± 0.17
HD 148387	6.20 ± 0.03	71.85 ± 1.34	TESS[5]	5016 ± 23	-0.08 ± 0.04	PASTEL[c]	35.72 ± 0.28
HD 163588	4.07 ± 0.02	37.23 ± 0.56	TESS[5]	4479 ± 18	-0.02 ± 0.03	PASTEL[c]	29.06 ± 0.12
HD 170693	1.57 ± 0.02	9.99 ± 0.32	TESS[5]	4447 ± 7	-0.41 ± 0.01	APOGEE[b]	11.06 ± 0.08
HD 176524	2.12 ± 0.04	18.29 ± 0.55	TESS[5]	4545 ± 29	-0.10 ± 0.05	PASTEL[c]	8.66 ± 0.23
HD 180711	4.77 ± 0.04	43.40 ± 0.65	TESS[5]	4841 ± 15	-0.15 ± 0.02	PASTEL[c]	33.35 ± 0.16
HD 181984	3.79 ± 0.03	33.50 ± 0.52	TESS[5]	4443 ± 21	0.11 ± 0.03	PASTEL[c]	21.67 ± 0.30
HD 28292	4.15 ± 0.04	34.95 ± 0.96	K2[6]	4519 ± 33	-0.12 ± 0.04	PASTEL[c]	16.80 ± 0.10
HD 31539	1.48 ± 0.10	9.38 ± 1.01	K2[6]	4210 ± 50	-0.32 ± 0.05	PASTEL[c]	6.87 ± 0.20

Notes. Asteroseismic references: 1: Guzik et al. (2016), 2: Lund et al. (2025), 3: Grundahl et al. (2017), 4: Teixeira et al. (2009), 5: Hon et al. (2022), 6: Pope et al. (2019).
Spectroscopic references: a: Soubiran et al. (2024), b: Abdurro'uf et al. (2022), c: Soubiran et al. (2022).

when the flagged baselines correspond to the shortest ones. The concerned observations are indicated in table 1 by an asterisk.

Among the 19 stars in our observed sample, 10 were observed at least twice. The individual analysis, between dates and instruments, allows us to validate the coherence of the results, as presented in Figure 3 for the star HD161797A. The angular diameter measurements for each night in each band is available in table B.1. No specific bias was detected, but it should be noted that the larger uncertainties and lower number of baselines of SPICA data generate larger uncertainties in the estimation, thus a less reliable measure with this instrument.

Moreover, Figure 3 also shows the comparison of the estimations between the different instruments. We can see that the MIRC-X and MYSTIC results are very close to each other with small uncertainties. Despite their larger uncertainties, the SPICA estimations remain coherent within 2σ uncertainties. This result allows us to confidently consider using a fit based on all the data from the three instruments to determine the final stellar angular diameter.

The second step generates this final angular diameter, called the polychromatic diameter. All the data are used to adjust a model with one single limb-darkened diameter and three sets of (c, d) coefficients for the three bands. An example of the fit is shown in Figure 4. This polychromatic interferometric angular diameter (hereafter $\theta_{\rm G}$) will be the one we will refer to throughout the next sections. They are presented in Table 3. The uncertainties on these angular diameters were derived from the reduced χ^2 profile by using $\chi_r^2(\theta_{\rm G}) = \min(\chi_r^2)$. Since the oimodeler code has demonstrated to underestimate the observation errors, we use the following reduce χ_r^2: $\chi_r^2(\theta_{\rm G} + \Delta\theta_{\rm G}) = \min(\chi_r^2) + 1$, to take into account those underestimations.

4.2. Interferometric radius

We calculated the interferometric radius of the stars using $\theta_{\rm G}$ and the parallaxes from Gaia (Gaia Collaboration et al. 2023). We took the star distance (in pc) $d = \frac{1}{\Pi}$, with Π the Gaia DR3 parallax (in arcs), because the relative uncertainties in the parallaxes are small. We then calculated the interferometric radius ($R_{\rm inter}$) as follows:

$$R_{\rm inter} = \frac{7.478 \times 10^7 \; d \; \theta_{\rm G}}{R_\odot}, \tag{3}$$

with $\theta_{\rm G}$ in arcseconds (arcs), d in pc and the solar radius $R_\odot$ taken from the most recent estimations (Prša et al. 2016; Haberreiter et al. 2008).

Interferometric radius of each of the 19 stars is reported in Table 3. The standard deviations for the calculated parameters throughout the article are calculated following the classical propagation of uncertainties[4]

4.3. Asteroseismic radius

The calculation of the asteroseismic radius is performed following the classical radius scaling relations (Kjeldsen & Bedding 1995):

$$\frac{R_{\rm ast}}{R_\odot} = \left(\frac{\Delta\nu}{\Delta\nu_\odot}\right)^{-2} \left(\frac{\nu_{\max}}{\nu_{\max\odot}}\right) \left(\frac{T_{\rm eff}}{T_{\rm eff\odot}}\right)^{0.5}, \tag{4}$$

with $\Delta\nu_\odot$, $\nu_{\max\odot}$ and $T_{\rm eff\odot}$ being respectively the solar $\Delta\nu$, $\nu_{\max}$ and the effective temperature $T_{\rm eff}$. The asteroseismic references for the solar values are taken from the estimations of Pinsonneault et al. (2018). The $T_{\rm eff}$ are selected

[4] Here, for Equation 3, it corresponds to $\Delta R_{\rm inter} = \left|\frac{\partial R_{\rm inter}}{\partial d}\right| \Delta d + \left|\frac{\partial R_{\rm inter}}{\partial \theta_{\rm G}}\right| \Delta\theta_{\rm G}$, with $\Delta R_{\rm inter}$, Δd and $\Delta\theta_{\rm G}$ being the uncertainties on, respectively, $R_{\rm inter}$, d and $\theta_{\rm G}$.

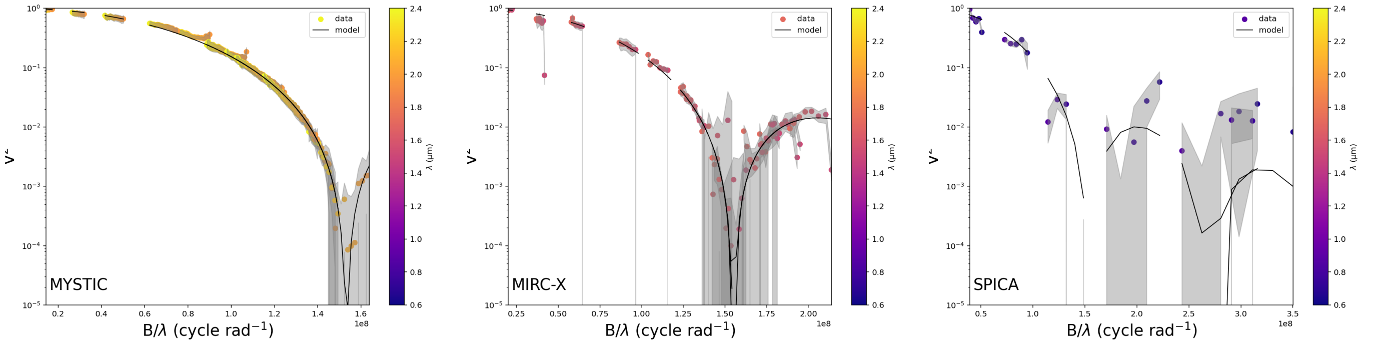

Fig. 2: Squared visibility (in log scale) as a function of spatial frequency for the star HD201091 taken during the night of the 14th of June 2025 with the MYSTIC (left), MIRC-X (center) and SPICA (right) instruments. The dots color code indicates the wavelength of the different spectral channels. The gray zones correspond to the 1σ uncertainties on the observed data. The black line corresponds to the square root LD fit with fixed Claret coefficients.

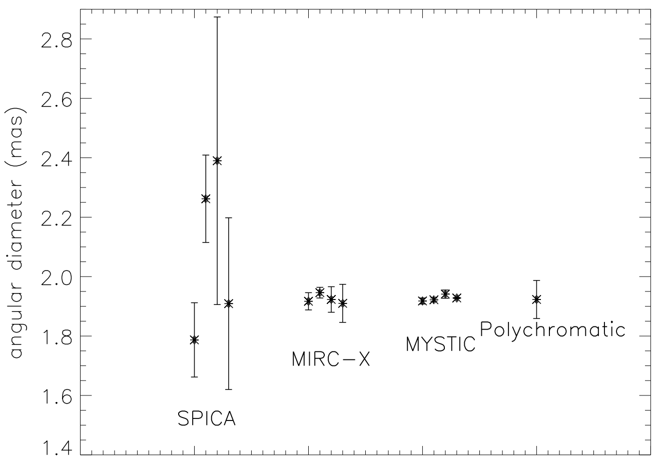

Fig. 3: Angular diameters extracted from the SPICA, MIRC-X and MYSTIC observations of the star HD161797A. For each instrument, the four estimations correspond, from left to right, to observation on July 4th 2024, April 23rd 2025, June 13th 2025 and August 18th 2025, respectively. The measurement was done with a square root LD fit and fixed Claret coefficients. The final polychromatic fit based on all the data is presented in the right part of the diagram.

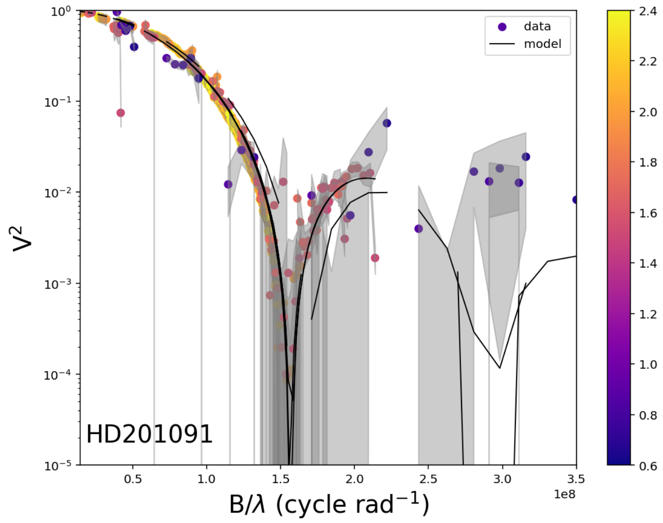

Fig. 4: SPICA, MIRC-X and MYSTIC squared visibilities in log scale as a function of spatial frequency for the star HD201091 during the night of the 14th of June 2025. The dots color code indicates the wavelength of the different spectral channels: yellow for MYSTIC, red for MIRC-X and blue for SPICA. The gray zones correspond to the 1σ uncertainties on the observed data. The black line corresponds to the square root LD fit with fixed Claret coefficients.

from various sources, depending on availability. First priority is the APOGEE catalog (Abdurro'uf et al. 2022), second the FGK benchmark stars catalog (Soubiran et al. 2024) and third the PASTEL catalog (Soubiran et al. 2016, 2022). These catalogs correspond to measurements from high-resolution spectroscopic observations, the PASTEL catalog aggregating results from several spectroscopic catalogs. The $T_{\rm eff}$ values and origin are indicated in Table 2, while the calculated $R_{\rm ast}$ and asteroseismic mass are given in Table 3.

5. Comparison of interferometric and asteroseismic radius

The comparison between $R_{\rm inter}$ and $R_{\rm ast}$ is shown in Table 3 and in Figure 5. We can see that the interferometric and asteroseismic radius are in agreement throughout the radius range, within 2σ uncertainty. This correlation between the two datasets is well demonstrated by the very high Pearson coefficient r = 0.992. The stars with K2 asteroseismic data seem to have a higher dispersion than the others, which is likely related to the difficulty to obtain reliable measurements with only 3 months of observations. The long-period oscillations of red giant stars (which can scale from hours to days) need long photometric light-curves in order to obtain a reliable result (Mosser et al. 2019) and this dispersion is the illustration of that limit rather than a true deviation.

The only star that exhibits a different behavior is HD185395 (θ Cyg) which possess excellent asteroseismic data with 4-year-long *Kepler* photometric light-curves and show a clear deviation from the interferometric measurements. We measure its radius as $R_{\rm inter} = 1.472 \pm 0.012 R_\odot$

Table 3: Polychromatic angular diameters of our stars (in mas), their asteroseismic and interferometric radius (in $R_\odot$) and their asteroseismic mass ($M_\odot$). The asteroseismic mass and radius were obtained with the classical asteroseismic scaling relations (Kjeldsen & Bedding, 1995).

HD number	θ_G (mas)	$R_{\rm inter}$ ($R_\odot$)	$R_{\rm ast}$ ($R_\odot$)	M ($M_\odot$)
HD 185395	0.743 ± 0.005	1.472 ± 0.012	1.679 ± 0.070	1.825 ± 0.048
HD 173667	0.963 ± 0.046	2.000 ± 0.100	2.093 ± 0.178	1.586 ± 0.188
HD 161797A	1.923 ± 0.064	1.724 ± 0.060	1.726 ± 0.029	1.160 ± 0.019
HD 10700	2.023 ± 0.028	0.794 ± 0.011	0.894 ± 0.049	1.123 ± 0.013
HD 22049	2.144 ± 0.45	0.742 ± 0.016	–	–
HD 160269A	0.646 ± 0.164	1.002 ± 0.257	1.024 ± 0.080	1.040 ± 0.049
HD 201091	1.666 ± 0.065	0.626 ± 0.025	–	–
HD 23249	2.313 ± 0.108	2.260 ± 0.110	2.161 ± 0.112	0.953 ± 0.076
HD 6186	1.965 ± 0.033	11.862 ± 0.320	13.822 ± 1.059	1.896 ± 0.154
HD 27371	2.341 ± 0.005	11.616 ± 0.123	10.461 ± 0.579	2.052 ± 0.119
HD 28305	2.562 ± 0.156	12.314 ± 0.845	11.275 ± 0.889	2.067 ± 0.220
HD 148387	3.493 ± 0.194	10.513 ± 0.667	10.287 ± 0.315	2.293 ± 0.060
HD 163588	3.044 ± 0.097	11.260 ± 0.404	11.688 ± 0.314	1.449 ± 0.037
HD 170693	2.035 ± 0.110	19.787 ± 1.220	21.002 ± 1.224	1.251 ± 0.067
HD 176524	1.783 ± 0.016	22.133 ± 0.779	21.319 ± 1.514	2.386 ± 0.203
HD 180711	3.334 ± 0.162	10.747 ± 0.573	10.313 ± 0.343	1.367 ± 0.052
HD 181984	2.301 ± 0.007	11.413 ± 0.195	12.080 ± 0.407	1.387 ± 0.0538
HD 28292	1.679 ± 0.034	10.742 ± 0.284	10.601 ± 0.534	1.124 ± 0.056
HD 31539	1.517 ± 0.038	23.735 ± 1.275	21.592 ± 5.371	1.208 ± 0.353

and $R_{\rm ast} = 1.679 \pm 0.070 \mathrm{R}_\odot$, which are clearly incompatible. A recent asteroseismic measurement from TESS data (Panetier et al. 2026) has found a lower radius value ($R_{\rm ast} = 1.658 \pm 0.115 \mathrm{R}_\odot$) compatible within 2σ uncertainties with our measurement. However, this result is obtained with 20 TESS sectors, which correspond to around 18 months of observations, thus to less resolved oscillation data than the one extracted from the 4-year long *Kepler* observations. Therefore, we considered preferentially the data from Guzik et al. (2016) that are more precise and accurate.

The deviation between asteroseismic and interferometric radii is present with all measurements we obtained with 6 observations during different nights in 2023 and 2024. It is also present with all instruments (SPICA, MIRC-X and MYSTIC), therefore the difference is not due to a technical or a specific observational problem during one of the nights. Several interferometric observations of θ Cyg have previously been performed with similar discrepant results (Ligi et al. 2012; White et al. 2013; Karovicova et al. 2022a). The only exception was the measurements performed by Boyajian et al. (2012) that are in agreement with asteroseismology, but this observation is done only in K-band with the CHARA Classic beam combiner for a star that is not resolved at this wavelength, thus it is more prone to biases. In fact, anomalies have previously been identified in this star visibilities through extensive interferometric studies (Ligi et al. 2012; White et al. 2013). A suspicion of binarity was put forward as a possible explanation for these abnormalities. Finally, Guzik et al. (2016) showed that, the asteroseismic results obtained from scaling relations can be in agreement with the interferometric observations if only the $\Delta\nu$ value is used and a lower $T_{\rm eff}$ is considered. Thus, the main discrepancy between the two techniques appears to be due to the high $T_{\rm eff}$ (6914 ± 33K) of this star that put it outside of the range where the scaling relations can be applied. At this temperature, the $\Delta\nu$ scaling relation is showing important deviations, as demonstrated by White et al. (2011a). It can be illustrated by the mass we obtain from the scaling relations ($M = 1.825 \pm 0.048 \mathrm{M}_\odot$) that put it outside the range of solar-like pulsators. This could also explain why this star is the only one showing a discrepancy between asteroseismic and interferometric measurements. A more thorough analysis of this target interferometric data would be necessary to understand its behavior, but that is beyond the scope of this paper.

In Figure 5, we also compare our result with previous studies (Huber et al. 2012; White et al. 2013; Baines et al. 2014; Johnson et al. 2014; Stokholm et al. 2019; Karovicova et al. 2022a,b). Those previous results showed an agreement between the asteroseismic and interferometric results for main-sequence and red giant stars until the clump, stars with radius around 10-12$R_\odot$. Here, we confirm that agreement with a robust polychromatic analysis and, thanks to our observations of evolved red giant stars, we extend the comparison for stars up to R $\approx 23 R_\odot$. This agreement seems in contradiction with the deviation of radii obtained with Gaia photometry and spectroscopy (hereafter fundamental radii) versus asteroseismic radii that was observed in the APOKASC3 data (Pinsonneault et al. 2025). A deviation between the two radii were indeed put forward for red giant branch stars with $\nu_{\rm max} < 20$ μHz, which correspond to stars with a typical stellar radius between 15 and 19$R_\odot$. This deviation is not seen in our direct measurements of angular diameter by interferometry, which demonstrate that classical asteroseismic estimations are reliable until 23$R_\odot$, the special cases of HD185395 having been discussed specifically. It is important to note that previous studies, using also *Kepler* data, indicate this type of deviation between asteroseismic and fundamental radii occurs at higher radius, with R $> 30 R_\odot$ (Zinn et al. 2019). However, this result was obtained using Gaia DR2 data, and with fewer stars compared to the APOKASC3 data which used Gaia DR3 data. APOKASC3 thus allows to reach a higher accuracy on the measured stellar radius. Therefore, this difference between our results and the fundamental radii is currently not resolved and deserve

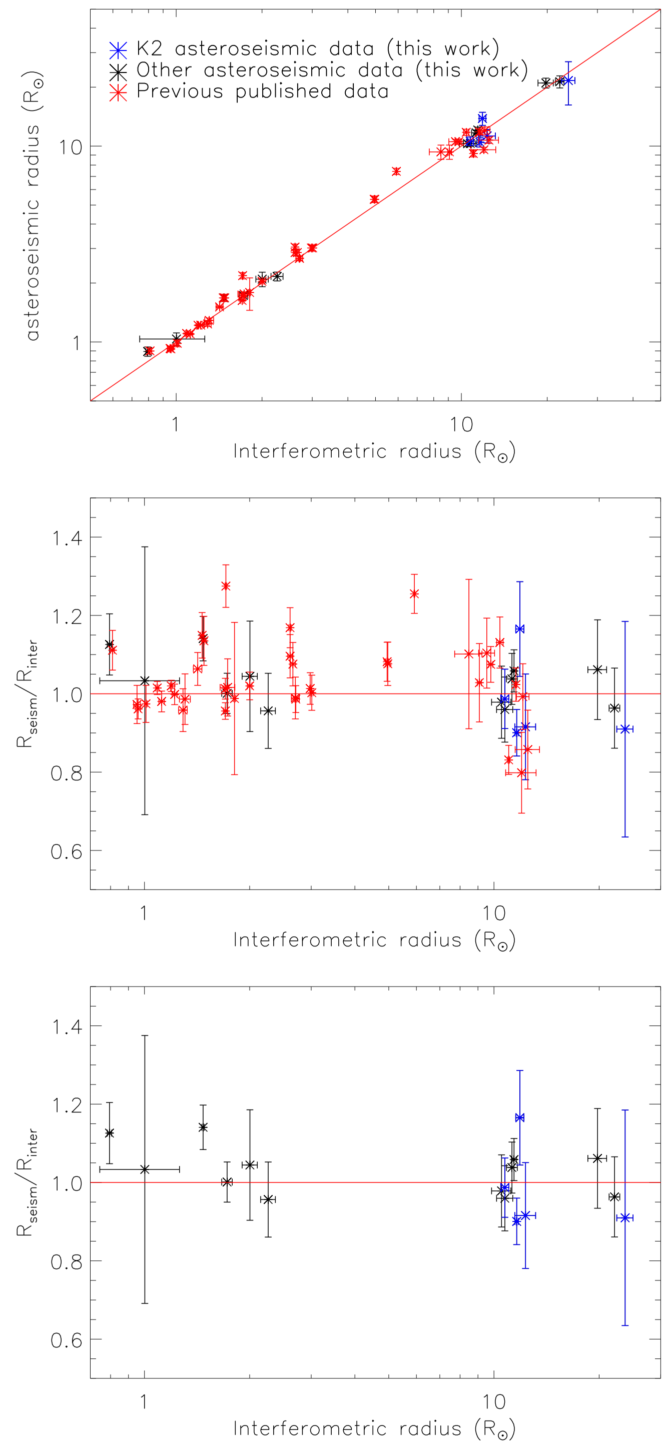

Fig. 5: *Top:* asteroseismic radius as a function of the interferometric radius from the polychromatic analysis. The blue and red stars correspond, respectively, to stars with K2 asteroseismic data and stars analyzed in previous publications. The red line shows what a perfect agreement between the two observation methods should exhibit. *Middle:* Ratio between the asteroseismic radius and the interferometric radius from the polychromatic analysis as a function of the same interferometric radius. *Bottom:* Same as middle panel but with only the polychromatic analysis from this work.

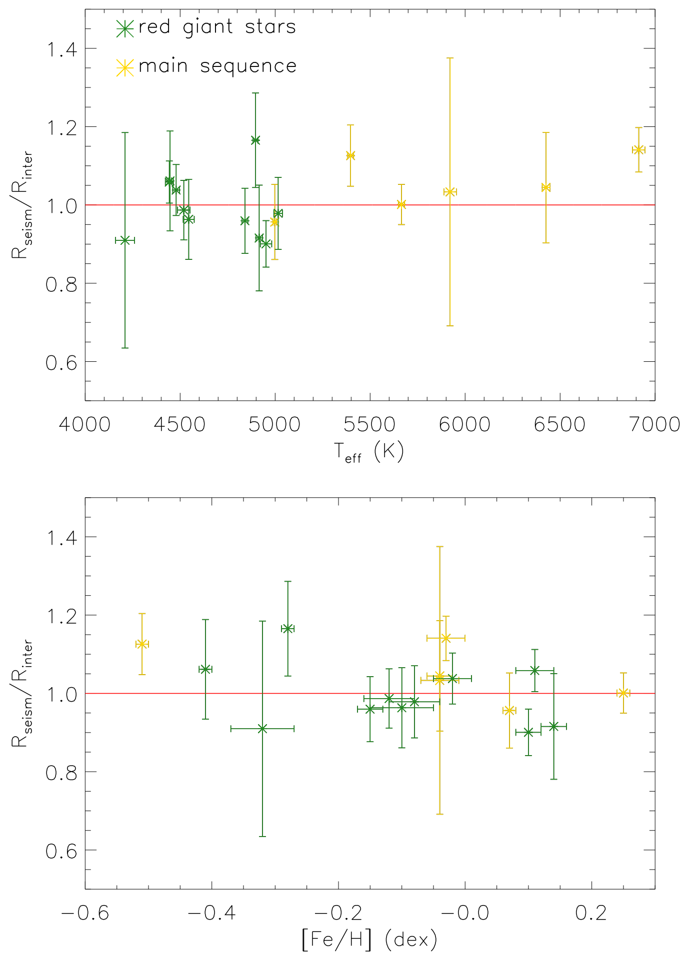

Fig. 6: Ratio between the asteroseismic radius and the interferometric radius from the polychromatic analysis as a function of the effective temperature T_{eff} (Top) and the metallicity [Fe/H] (Bottom). The yellow stars correspond to the main-sequence objects and the green stars to the red giant targets. The red line indicates a perfect agreement between the two observation methods.

a thorough investigation that is beyond the scope of this paper.

We investigated the influence of the T_{eff} and the metallicity (see Table 2) on the ratio between asteroseismic and interferometric radius. The results are plotted in Figure 6. The high T_{eff} value of HD185395 biases slightly the results towards a possible T_{eff} dependence but we already discuss the biases on that specific star previously. We performed a linear fit, removing HD185395, and found a small positive dependence with T_{eff} and negative dependence with metallicity but within 2σ uncertainties. Therefore we concluded that no clear dependence were discovered. This result is probably due to the too small sample and its lack of homogeneity that do not allow us to bring out significant dependencies. Thus, it highlights the necessity to continue the survey to obtain a more significant sized sample of stars and better constrain the scaling relations.

Table 4: Pearson correlation coefficients (Pearson's r) between the interferometric radius from polychromatic analysis and the asteroseismic radius obtained with different scaling relations.

Scaling relation	Pearson's r	χ^2
Kjeldsen & Bedding (1995)	0.992	0.939
White et al. (2011)	0.992	0.969
Guggenberger et al. (2017)	0.992	1.253
Bellinger (2019)	0.987	1.749
Li et al. (2022)	0.992	3.065

6. Disantengling the different scaling relations

Several modifications to the classical scaling relations (Kjeldsen & Bedding 1995) used in the previous section have been proposed to take into account the different characteristics of stars. We present below the comparison of these asteroseismic radius estimations with our interferometric results. The results are presented in Figure 7 and Table 5, while the different Pearson correlation coefficients between the asteroseismic and interferometric radius are reported in Table 4.

6.1. White et al. (2011b) scaling relation

Using ASTEC models (Christensen-Dalsgaard 2008), White et al. (2011b) demonstrated that one of the scaling relations, which relates the stellar density and the large frequency separation $\Delta\nu$, shows a deviation as a function of the effective temperature of the model. Thus, a modification to the $\Delta\nu$ scaling relation was proposed for stars with 4700 K $< T_{\rm eff} <$ 6700K (excluding main-sequence stars with M $< 1.2 M_\odot$):

$$\frac{\rho}{\rho_\odot} = \left(\frac{\Delta\nu}{\Delta\nu_\odot}\right)^2 (f(T_{\rm eff}))^{-2}, \quad (5)$$

with ρ being the mean density of the star, $\rho_\odot$ the mean density of the Sun and $f(T_{\rm eff})$ corresponding to:

$$f(T_{\rm eff}) = -4.29\left(\frac{T_{\rm eff}}{10^4{\rm K}}\right)^2 + 4.84\left(\frac{T_{\rm eff}}{10^4{\rm K}}\right) - 0.35. \quad (6)$$

The scaling relation is now written as:

$$\frac{R_{\rm ast}}{R_\odot} = \left(\frac{\Delta\nu}{\Delta\nu_\odot}\right)^{-2} (f(T_{\rm eff}))^2 \left(\frac{\nu_{\rm max}}{\nu_{\rm max\odot}}\right)\left(\frac{T_{\rm eff}}{T_{\rm eff\odot}}\right)^{0.5}. \quad (7)$$

The new estimation of the asteroseismic radius is compared with the interferometric one and presented in Figure 7. The asteroseismic and interferometric values appear to be closer to each other, but it has practically no effect on the Pearson correlation coefficient, which is already very high, and to the χ^2.

It is interesting to note that HD185395 is not in the validity domain of the scaling relation modification due to its high $T_{\rm eff}$. However, if it were the case, its asteroseismic radius would fall at $R_{\rm ast} = 1.501 \pm 0.062 R_\odot$, which is less than 2σ away from its $R_{\rm inter}$ estimation. The high $T_{\rm eff}$ of the star would thus allow for a better agreement with this modification of the scaling relations. This was already pointed out by Karovicova et al. (2022a) who suggested that the addition of a temperature dependence in the scaling relations would reduce the discrepancy between those two measurements for that target. In that situation, assuming that modification to the relation can be extended towards higher-$T_{\rm eff}$ stars, the apparent disagreement for θ Cyg may not need another exterior explanation.

6.2. Guggenberger et al. (2016, 2017) scaling relation

Using the YREC stellar evolution code (Demarque et al. 2008), Guggenberger et al. (2016) performed a different calibration of the scaling relation taking into account the metallicity ([Fe/H]) and $T_{\rm eff}$ dependence from the models. They propose the following modification of the solar reference value:

$$\Delta\nu_{\rm ref} = (0.64[{\rm F}e/H]+1.78){\rm e}^{\rm A}\cos({\rm B})+0.66[{\rm F}e/H]+134.92, \quad (8)$$

with $A = \frac{(-0.55[Fe/H]+1.23)T_{\rm eff}}{10^4{\rm K}}$ and $B = \frac{22.21 T_{\rm eff}}{10^4{\rm K}} + 0.48[Fe/H] + 0.12$. $\Delta\nu_{\rm ref}$ is the value replacing the solar reference value for the large separation ($\Delta\nu_\odot$) in the scaling relations (Eq. 7). Guggenberger et al. (2017) extended the proposed modification with the addition of a mass dependence for stars with $\nu_{\rm max} < 170\mu$Hz following this formula:

$$\Delta\nu_{\rm ref} = 124.72 + 2.23M + \frac{17.61}{\nu_{\rm max}} + 0.73\sqrt{\nu_{\rm max}} - 0.02\nu_{\rm max} - 0.93[{\rm Fe/H}], \quad (9)$$

with M the stellar mass.

The asteroseismic radii are then computed with these new reference values, the mass from the classical scaling relations, and the metallicity from the same reference as the $T_{\rm eff}$ for the different stars. The results are presented in Figure 7. The results, showed in Figure 7, appears to improve the dispersion in the main sequence for some targets, specifically HD185395. It confirms that taking into account the mass and metallicity dependence for that target is sufficient to explain the discrepancy between the two observation methods. However, it does not seem to improve the overall result, which is confirmed by a similar Pearson correlation coefficient and χ^2 as for the classical scaling relations.

6.3. Bellinger (2019) scaling relation.

Using a sample of main-sequence and subgiant stars as calibrators, Bellinger (2019) proposed new scaling relations for stellar mass, radius, and age taking into account metallicity dependence. The calibration is made with measurements performed with the *Stellar Parameters in an Instant* (SPI, Bellinger et al. 2016) pipeline, using machine learning that connects their observations to theoretical models. The new scaling relations is written as follows:

$$\frac{R_{\rm ast}}{R_\odot} = \left(\frac{\Delta\nu}{\Delta\nu_\odot}\right)^{-1.129}\left(\frac{\nu_{\rm max}}{\nu_{\rm max\odot}}\right)^{0.305}\left(\frac{T_{\rm eff}}{T_{\rm eff\odot}}\right)^{0.312}\exp\left([{\rm Fe/H}]\right)^{0.1}. \quad (10)$$

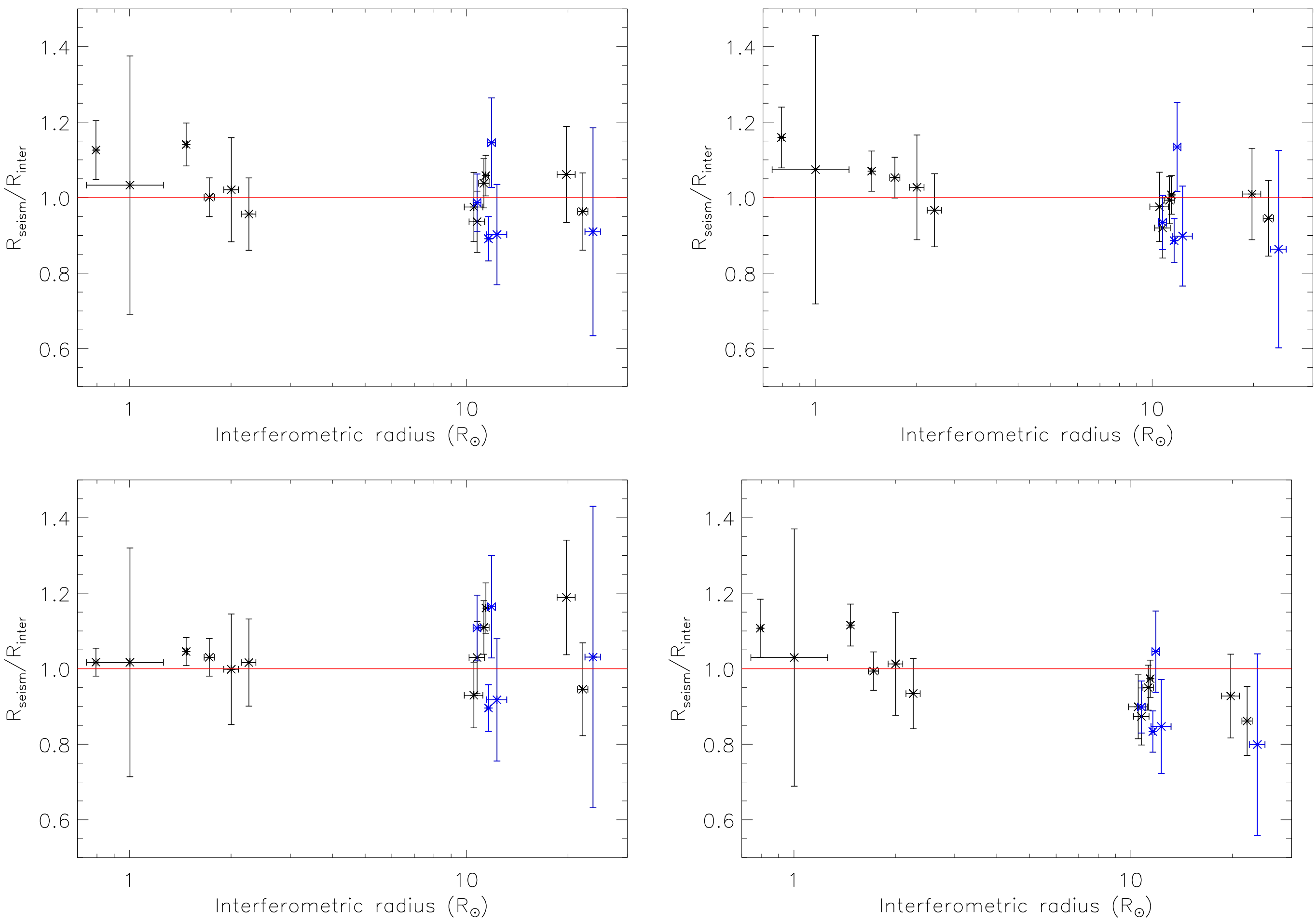

Fig. 7: Ratio between the asteroseismic radius and the interferometric radius from polychromatic analysis as a function of the same interferometric radius. The blue stars correspond to stars with K2 asteroseismic data. From top-left to bottom-right, the asteroseismic radius were derived from White et al. (2011b), Guggenberger et al. (2017), Bellinger (2019) and Li et al. (2022) scaling relations, respectively.

Table 5: Asteroseismic radius (in $R_\odot$) calculated from different modified asteroseismic scaling relations.

HD number	$R_{\rm ast}$ (White) ($R_\odot$)	$R_{\rm ast}$ (Guggenberger) ($R_\odot$)	$R_{\rm ast}$ (Bellinger) ($R_\odot$)	$R_{\rm ast}$ (Li) ($R_\odot$)
HD 185395	1.679 ± 0.070	1.575 ± 0.065	1.539 ± 0.042	1.642 ± 0.068
HD 173667	2.046 ± 0.174	2.058 ± 0.175	2.000 ± 0.193	2.029 ± 0.171
HD 161797A	1.726 ± 0.029	1.815 ± 0.031	1.776 ± 0.025	1.713 ± 0.028
HD 10700	0.894 ± 0.049	0.921 ± 0.051	0.808 ± 0.018	0.879 ± 0.048
HD 22049	–	–	–	–
HD 160269A	1.036 ± 0.077	1.077 ± 0.080	1.019 ± 0.042	1.032 ± 0.076
HD 201091	–	–	–	–
HD 23249	2.161 ± 0.112	2.184 ± 0.113	2.297 ± 0.149	2.111 ± 0.108
HD 6186	13.585 ± 1.041	13.453 ± 1.031	13.807 ± 1.235	12.398 ± 0.944
HD 27371	10.352 ± 0.572	10.292 ± 0.569	10.407 ± 0.610	9.684 ± 0.532
HD 28305	11.108 ± 0.876	11.062 ± 0.872	11.299 ± 1.219	10.430 ± 0.815
HD 148387	10.253 ± 0.314	10.257 ± 0.314	9.773 ± 0.286	9.453 ± 0.290
HD 163588	11.688 ± 0.314	11.184 ± 0.301	12.491 ± 0.350	10.697 ± 0.287
HD 170693	21.002 ± 1.224	19.977 ± 1.165	23.523 ± 1.552	18.354 ± 1.065
HD 176524	21.319 ± 1.514	20.927 ± 1.486	20.929 ± 1.985	19.069 ± 1.349
HD 180711	10.060 ± 0.335	9.883 ± 0.329	11.065 ± 0.440	9.388 ± 0.311
HD 181984	12.080 ± 0.407	11.496 ± 0.388	13.247 ± 0.534	11.110 ± 0.373
HD 28292	10.601 ± 0.534	10.037 ± 0.506	11.900 ± 0.622	9.654 ± 0.485
HD 31539	21.592 ± 5.371	20.499 ± 5.099	24.467 ± 8.161	18.967 ± 4.686

The asteroseismic radius for the stars of our sample are then calculated, taking the metallicity from the same spectroscopic catalog as described in Section 4.3. The results are presented in Figure 7. We can see that the coherence between the asteroseismic and interferometric radius seems to be better for main-sequence stars, but it has a negligible impact on the Pearson correlation coefficient and produce a slight increase in the χ^2. This result is due to the higher dispersion we can observe for red giant stars, which is coherent, since the scaling relations were calibrated mainly with main sequence objects. However, these results show that this calibration is valid even for evolved red giants.

It is interesting to highlight the case of HD10700 (τ Ceti) which has the lowest metallicity values and radius in our sample. Using this scaling relation, we can see in Figure 7 that it makes the difference between R_{ast} and R_{inter} negligible, a clear improvement with respect to the classical scaling relation for this target. The same case can be argued for HD185395 as for the use of the precedent relation. This result enhances the necessity of taking into account the metallicity influence on the scaling relations and to perform its proper calibration. It also put forward the necessity to perform detailed stellar modelisation of those stars.

6.4. Li et al. (2022) scaling relation.

Using stellar parameters derived from observations of more than 3000 red giants, models from the MESA evolution code (Paxton et al. 2011, 2013, 2015, 2018) and GYRE oscillation code (Townsend & Teitler 2013), Li et al. (2022) calibrated new scaling relations for red giants. This corrected scaling relation for the stellar radius is the following:

$$\frac{R_{\text{ast}}}{R_{\odot}} = \left(\frac{\Delta\nu}{\Delta\nu_{\odot}}\right)^{-1.972} \left(\frac{\nu_{\max}}{\nu_{\max\odot}}\right) \left(\frac{T_{\text{eff}}}{T_{\text{eff}\odot}}\right)^{0.459} (10^{[\text{Fe/H}]})^{0.117}. \quad (11)$$

We applied this scaling relation for our sample, taking the metallicity from the same spectroscopic catalog as described in Section 4.3. The results are presented in Figure 7. The results show no difference from the classical scaling relation for main-sequence stars, which is coherent with the fact that this scaling relation was calibrated with red giant objects. This is illustrated by the Pearson correlation coefficient, similar to the classical scaling relation (Eq. 7). However, even if some changes appear for red giants with lower asteroseismic radii giving the impression of a decrease a a function of the radius, the correlation between the asteroseismic and interferometric data is not modified. Indeed, restricting to red giants only, the Pearson correlation coefficient (r = 0.975) is equivalent to the one for the classical scaling relation (r = 0.973). Only the χ^2 is affected positively, even if we restrict it to the red giants. It brings interrogations to the interest of this relation but the number of stars and the uncertain results does not allow us to reach a firm conclusion.

All of these results indicates that the correlation between the asteroseismic scaling relations and interferometric data in the radius range we considered in this work is high enough that modifications on these scaling relations will have a negligible impact. The only notable modifications occurs for main-sequence stars with unusual T_{eff} or metallicity values, bringing the asteroseismic and interferometric results compatible with some of the scaling relation modifications. This, however, does not affect the overall correlation between the two observation methods. Thus, it is not possible to conclude on the improvement brought by the different modifications to the scaling relations, therefore emphasizing the need to complete the sample.

7. Conclusion

In this paper, we present the first simultaneous interferometric observations in three bands (R, H, and K) for solar-mass stars with asteroseismoic data. So far, 19 stars were observed with SPICA, MIRC-X, and MYSTIC instruments on the CHARA Array between 2023 and 2025. For each star, we estimated angular diameters, adopting a square root LD law, and demonstrated the coherence between the different instruments and the different nights. We computed the interferometric radius using Gaia parallaxes and compared it with the one obtained with asteroseismic scaling relations. We showed that the asteroseismic and interferometric radii are consistent with each other for our sample, covering a range between $0.8R_{\odot}$ and $23R_{\odot}$. We put forward a disagreement for stars above $18R_{\odot}$ between our result and the one analyzing the consistency of asteroseismic radii and radii obtained with APOGEE and Gaia data (Pinsonneault et al. 2025). This difference is not present for previous comparisons (Zinn et al. 2023) and is currently unexplained. We also analyze the T_{eff} and metallicity dependence of the ratio between asteroseismic and interferometric radii and reach no significant conclusion with the current sample. Finally, we performed an analysis of the different proposed modifications to the asteroseismic scaling relations and demonstrated that, they do not significantly change the agreement with interferometric measurements, at the exceptions of targets with particularly high T_{eff} or low metallicity.

This work confirms and extends previous analysis about the reliability of asteroseismic scaling relations. We extended the compatibility of the radius above the clump, towards R = $23R_{\odot}$, which was previously contested. In order to test the limits of the scaling relations, it would be necessary to extend the interferometric observations towards stars with R > $30R_{\odot}$, since this is where all studies are in agreement about the limits of their reliability. We also put forward that the different proposed modifications to the scaling relations mainly do not affect importantly the agreement with interferometric observations. Though, it is difficult to reach a conclusion with these modifications since the agreement between asteroseismic and interferometric data is already very good with the classical scaling relation. Therefore, every modifications to the scaling relations will not be able to improve significantly the correlation between the measurements from the two methods. It would be necessary to extend the study towards more diverse T_{eff}, metallicity, evolutionary status and higher radius in order to highlight a clear difference between the different scaling relations. In order to strengthen all those results, it will be necessary to continue to observe stars with asteroseismic observations as is schedule for the ISSP program. It will increase the sample of stars to obtain a statistically significant sample and constrain the scaling relations taking into account the influence of the mass, metallicity and evolutionary status on those relation. The comparison with different asteroseismic results from different scaling relations would then also lead to clearer conclusions. These results are likely to be achieved in the near future through the continuation of the ISSP program during 2026 and 2027.

Acknowledgements. This project has received funding from the European Research Council (ERC) under the European Union's

Horizon 2020 research and innovation programme (Grant agreement No. 101019653). SPICA has been funded by CNRS, Observatoire de la Côte d'Azur, Université Côte d'Azur, Région Sud, and the University of Aarhus. This work is based on observations obtained with the Georgia State University Center for High Angular Resolution Astronomy Array at Mount Wilson Observatory.
The CHARA Array is supported by the National Science Foundation under Grant No. AST-2034336 and AST-2407956. Institutional support has been provided from the GSU College of Arts and Sciences, Office of the Provost, and Office of the Vice President for Research and Economic Development.
MIRC-X has been built with funds from an ERC Starting Grant (Grant Agreement No. 639889) and an STFC equipment grant ST/X005143/1.
We thank the CHARA Array staff members C.D. Farrington, B. Flores, K. Kubiak, O. Majoinen, H.D. Rentiera and N.L. Vargas for their huge contribution during the observations.
S.K acknowledges funding for MIRC-X received funding from the European Research Council (ERC) under the European Union's Horizon 2020 research and innovation programme (Starting Grant No. 639889 and Consolidated Grant No. 101003096). J.D.M acknowledges funding for the development of MIRC-X (NASA-XRP NNX16AD43G, NSF-AST 2009489) and MYSTIC (NSF-ATI 1506540, NSF-AST 1909165).
O. Creevey thanks T. Boyajian and W. Chaplin for their contributions to the main-sequence stars target list.
A.G acknowledges support from the Agencia Nacional de Investigación y Desarrollo (ANID) through FONDECYT Regular grant 1241073.
TM acknowledges financial support from Belspo for contract PRODEX PLATO mission development.
R. Szabó acknowledges the SNN-147362 and KKP-137523 grants of the Hungarian National Research, Development and Innovation Office, as well as the Lendület "Momentum" program of the Hungarian Academy of Sciences, project No. LP2025-14.
This work has made use of data from the European Space Agency (ESA) mission *Gaia* (`https://www.cosmos.esa.int/gaia`), processed by the *Gaia* Data Processing and Analysis Consortium (DPAC, `https://www.cosmos.esa.int/web/gaia/dpac/consortium`). Funding for the DPAC has been provided by national institutions, in particular the institutions participating in the *Gaia* Multilateral Agreement.

References

Abdurro'uf, Accetta, K., Aerts, C., et al. 2022, ApJS, 259, 35
Adassuriya, J., Ganesh, S., Gutiérrez, J. L., et al. 2021, MNRAS, 502, 541
Addison, B. C., Wright, D. J., Nicholson, B. A., et al. 2021, MNRAS, 502, 3704
Anugu, N., Le Bouquin, J.-B., Monnier, J. D., et al. 2020, AJ, 160, 158
Appourchaux, T., Chaplin, W. J., García, R. A., et al. 2012, A&A, 543, A54
Baglin, A., Auvergne, M., Barge, P., et al. 2006, in ESA Special Publication, Vol. 1306, The CoRoT Mission Pre-Launch Status - Stellar Seismology and Planet Finding, ed. M. Fridlund, A. Baglin, J. Lochard, & L. Conroy, 33
Baglin, A. & Michel, E. 2015, in European Physical Journal Web of Conferences, Vol. 101, European Physical Journal Web of Conferences (EDP), 06002
Baines, E. K., Armstrong, J. T., Schmitt, H. R., et al. 2014, ApJ, 781, 90
Ball, W. H., Chaplin, W. J., Nielsen, M. B., et al. 2020, MNRAS, 499, 6084
Bazot, M., Campante, T. L., Chaplin, W. J., et al. 2012, A&A, 544, A106
Bedding, T. R., Kjeldsen, H., Arentoft, T., et al. 2007, ApJ, 663, 1315
Belkacem, K., Goupil, M. J., Dupret, M. A., et al. 2011, A&A, 530, A142
Bellinger, E. P. 2019, MNRAS, 486, 4612
Bellinger, E. P., Angelou, G. C., Hekker, S., et al. 2016, ApJ, 830, 31
Benbakoura, M., Gaulme, P., McKeever, J., et al. 2021, A&A, 648, A113
Benomar, O., Baudin, F., Campante, T. L., et al. 2009, A&A, 507, L13
Borucki, W. J., Koch, D., Basri, G., et al. 2010, Science, 327, 977
Bourges, L., Mella, G., Lafrasse, S., et al. 2017, VizieR Online Data Catalog: JMMC Stellar Diameters Catalogue - JSDC. Version 2 (Bourges+, 2017), VizieR On-line Data Catalog: II/346. Originally published in: 2014ASPC..485..223B
Boyajian, T. S., McAlister, H. A., van Belle, G., et al. 2012, ApJ, 746, 101
Brogaard, K., Hansen, C. J., Miglio, A., et al. 2018, MNRAS, 476, 3729
Campante, T. L., Corsaro, E., Lund, M. N., et al. 2019, ApJ, 885, 31
Carrier, F. & Eggenberger, P. 2006, Mem. Soc. Astron. Italiana, 77, 326
Carrier, F., Eggenberger, P., & Bouchy, F. 2005a, A&A, 434, 1085
Carrier, F., Eggenberger, P., D'Alessandro, A., & Weber, L. 2005b, New A, 10, 315
Chaplin, W. J., Lund, M. N., Handberg, R., et al. 2015, PASP, 127, 1038
Chaplin, W. J., Serenelli, A. M., Miglio, A., et al. 2020, Nature Astronomy, 4, 382
Chelli, A., Duvert, G., Bourgès, L., et al. 2016, A&A, 589, A112
Chontos, A., Huber, D., Berger, T. A., et al. 2021, ApJ, 922, 229
Christensen-Dalsgaard, J. 2008, Ap&SS, 316, 13
Claret, A. & Bloemen, S. 2011, A&A, 529, A75
de Laverny, P., Recio-Blanco, A., Navarrete, C., Palicio, P. A., & Spitoni, E. 2026, A&A, 711, A54
Demarque, P., Guenther, D. B., Li, L. H., Mazumdar, A., & Straka, C. W. 2008, Ap&SS, 316, 31
Duvert, G., Young, J., & Hummel, C. A. 2017, A&A, 597, A8
Ebrahimkutty, N., Gent, M. R., Mourard, D., et al. 2024, A&A, 691, A207
Eisenhauer, F., Monnier, J. D., & Pfuhl, O. 2023, ARA&A, 61, 237
Gaia Collaboration, Vallenari, A., Brown, A. G. A., et al. 2023, A&A, 674, A1
Gaulme, P., McKeever, J., Jackiewicz, J., et al. 2016, ApJ, 832, 121
GRAVITY Collaboration, Abuter, R., Accardo, M., et al. 2017, A&A, 602, A94
Grunblatt, S. K., Huber, D., Gaidos, E., et al. 2019, AJ, 158, 227
Grundahl, F., Fredslund Andersen, M., Christensen-Dalsgaard, J., et al. 2017, ApJ, 836, 142
Guggenberger, E., Hekker, S., Angelou, G. C., Basu, S., & Bellinger, E. P. 2017, MNRAS, 470, 2069
Guggenberger, E., Hekker, S., Basu, S., & Bellinger, E. 2016, MNRAS, 460, 4277
Gupta, A., Verma, K., Kjeldsen, H., et al. 2025, MNRAS, 544, 3428
Guzik, J. A., Houdek, G., Chaplin, W. J., et al. 2016, ApJ, 831, 17
Haberreiter, M., Schmutz, W., & Kosovichev, A. G. 2008, ApJ, 675, L53
Haubois, X., Bernaud, P., Mella, G., et al. 2014, in Society of Photo-Optical Instrumentation Engineers (SPIE) Conference Series, Vol. 9146, Optical and Infrared Interferometry IV, ed. J. K. Rajagopal, M. J. Creech-Eakman, & F. Malbet, 91460O
Hon, M., Kuszlewicz, J. S., Huber, D., Stello, D., & Reyes, C. 2022, AJ, 164, 135
Huber, D., Chaplin, W. J., Chontos, A., et al. 2019, AJ, 157, 245
Huber, D., Chaplin, W. J., Christensen-Dalsgaard, J., et al. 2013, ApJ, 767, 127
Huber, D., Ireland, M. J., Bedding, T. R., et al. 2012, ApJ, 760, 32
Huber, D., Zinn, J., Bojsen-Hansen, M., et al. 2017, ApJ, 844, 102
Jiang, C., Bedding, T. R., Stassun, K. G., et al. 2020, ApJ, 896, 65
Johnson, J. A., Huber, D., Boyajian, T., et al. 2014, ApJ, 794, 15
Kallinger, T., Mosser, B., Hekker, S., et al. 2010a, A&A, 522, A1
Kallinger, T., Weiss, W. W., Barban, C., et al. 2010b, A&A, 509, A77
Karovicova, I., White, T. R., Nordlander, T., et al. 2022a, A&A, 658, A47
Karovicova, I., White, T. R., Nordlander, T., et al. 2022b, A&A, 658, A48
Kjeldsen, H. & Bedding, T. R. 1995, A&A, 293, 87
Labeyrie, A. 1975, ApJ, 196, L71
Lagarde, N., Miglio, A., Eggenberger, P., et al. 2015, A&A, 580, A141
Li, T., Li, Y., Bi, S., et al. 2022, ApJ, 927, 167
Ligi, R., Mourard, D., Lagrange, A. M., et al. 2012, A&A, 545, A5
Liu, Z., Yang, W., Bi, S., et al. 2014, ApJ, 780, 152
Lund, M. N., Basu, S., Silva Aguirre, V., et al. 2016, MNRAS, 463, 2600
Lund, M. N., Chontos, A., Grundahl, F., et al. 2025, A&A, 701, A285
Lund, M. N., Knudstrup, E., Silva Aguirre, V., et al. 2019, AJ, 158, 248
Lund, M. N., Silva Aguirre, V., Davies, G. R., et al. 2017, ApJ, 835, 172

Malla, S. P., Stello, D., Huber, D., et al. 2020, MNRAS, 496, 5423
Mathur, S., Metcalfe, T. S., Woitaszek, M., et al. 2012, ApJ, 749, 152
Meilland, A., Scheuck, M., Varga, J., Matter, A., & Millour, F. 2024, in Society of Photo-Optical Instrumentation Engineers (SPIE) Conference Series, Vol. 13095, Optical and Infrared Interferometry and Imaging IX, ed. J. Kammerer, S. Sallum, & J. Sanchez-Bermudez, 130952W
Metcalfe, T. S., Creevey, O. L., Doğan, G., et al. 2014, ApJS, 214, 27
Metcalfe, T. S., van Saders, J. L., Basu, S., et al. 2020, ApJ, 900, 154
Miglio, A., Chiappini, C., Morel, T., et al. 2013, in European Physical Journal Web of Conferences, Vol. 43, European Physical Journal Web of Conferences (EDP), 03004
Mosser, B., Michel, E., Samadi, R., et al. 2019, A&A, 622, A76
Mourard, D., B. P. B. C. C. A. D. J. 2026, A&A submitted
Nielsen, M. B., Ball, W. H., Standing, M. R., et al. 2020, A&A, 641, A25
Panetier, E., Hookway, G. T., Corsaro, E., et al. 2026, arXiv e-prints, arXiv:2605.14713
Paxton, B., Bildsten, L., Dotter, A., et al. 2011, ApJS, 192, 3
Paxton, B., Cantiello, M., Arras, P., et al. 2013, ApJS, 208, 4
Paxton, B., Marchant, P., Schwab, J., et al. 2015, ApJS, 220, 15
Paxton, B., Schwab, J., Bauer, E. B., et al. 2018, ApJS, 234, 34
Pinsonneault, M. H., Elsworth, Y. P., Tayar, J., et al. 2018, ApJS, 239, 32
Pinsonneault, M. H., Zinn, J. C., Tayar, J., et al. 2025, ApJS, 276, 69
Pope, B. J. S., White, T. R., Farr, W. M., et al. 2019, ApJS, 245, 8
Prša, A., Harmanec, P., Torres, G., et al. 2016, AJ, 152, 41
Rauer, H., Aerts, C., Cabrera, J., et al. 2025, Experimental Astronomy, 59, 26
Ricker, G. R., Winn, J. N., Vanderspek, R., et al. 2015, Journal of Astronomical Telescopes, Instruments, and Systems, 1, 014003
Rodrigues, T. S., Bossini, D., Miglio, A., et al. 2017, MNRAS, 467, 1433
Sahlholdt, C. L. & Silva Aguirre, V. 2018, MNRAS, 481, L125
Salsi, A., Nardetto, N., Mourard, D., et al. 2020, A&A, 640, A2
Salsi, A., Nardetto, N., Mourard, D., et al. 2021, A&A, 652, A26
Setterholm, B. R., Monnier, J. D., Le Bouquin, J.-B., et al. 2023, Journal of Astronomical Telescopes, Instruments, and Systems, 9, 025006
Sharma, S., Stello, D., Bland-Hawthorn, J., Huber, D., & Bedding, T. R. 2016, ApJ, 822, 15
Silva Aguirre, V., Basu, S., Brandão, I. M., et al. 2013, ApJ, 769, 141
Silva Aguirre, V., Casagrande, L., Basu, S., et al. 2012, ApJ, 757, 99
Soubiran, C., Brouillet, N., & Casamiquela, L. 2022, A&A, 663, A4
Soubiran, C., Creevey, O. L., Lagarde, N., et al. 2024, A&A, 682, A145
Soubiran, C., Le Campion, J.-F., Brouillet, N., & Chemin, L. 2016, A&A, 591, A118
Stello, D., Zinn, J., Elsworth, Y., et al. 2017, ApJ, 835, 83
Stokholm, A., Nissen, P. E., Silva Aguirre, V., et al. 2019, MNRAS, 489, 928
Teixeira, T. C., Kjeldsen, H., Bedding, T. R., et al. 2009, A&A, 494, 237
Townsend, R. H. D. & Teitler, S. A. 2013, MNRAS, 435, 3406
Van Eylen, V., Dai, F., Mathur, S., et al. 2018, MNRAS, 478, 4866
Viani, L. S., Basu, S., Chaplin, W. J., Davies, G. R., & Elsworth, Y. 2017, ApJ, 843, 11
White, T. R., Bedding, T. R., Stello, D., et al. 2011a, ApJ, 742, L3
White, T. R., Bedding, T. R., Stello, D., et al. 2011b, ApJ, 743, 161
White, T. R., Huber, D., Maestro, V., et al. 2013, MNRAS, 433, 1262
Yu, J., Huber, D., Bedding, T. R., et al. 2018, ApJS, 236, 42
Zinn, J. C., Pinsonneault, M. H., Bildsten, L., & Stello, D. 2023, MNRAS, 525, 5540
Zinn, J. C., Pinsonneault, M. H., Huber, D., et al. 2019, ApJ, 885, 166
Zwintz, K., Aerts, C., Tkachenko, A., et al. 2026, arXiv e-prints, arXiv:2604.04042

Appendix A: Polychromatic Angular diameter fit

The polychromatic fit for the 19 observed stars in this analysis is shown in Figure A.1

Appendix B: Angular diameters for R,H,K bands separately and each observations

The angular diameter fits for each observations separately and each spectral bands (R,H,K) are shown in Table B.1.

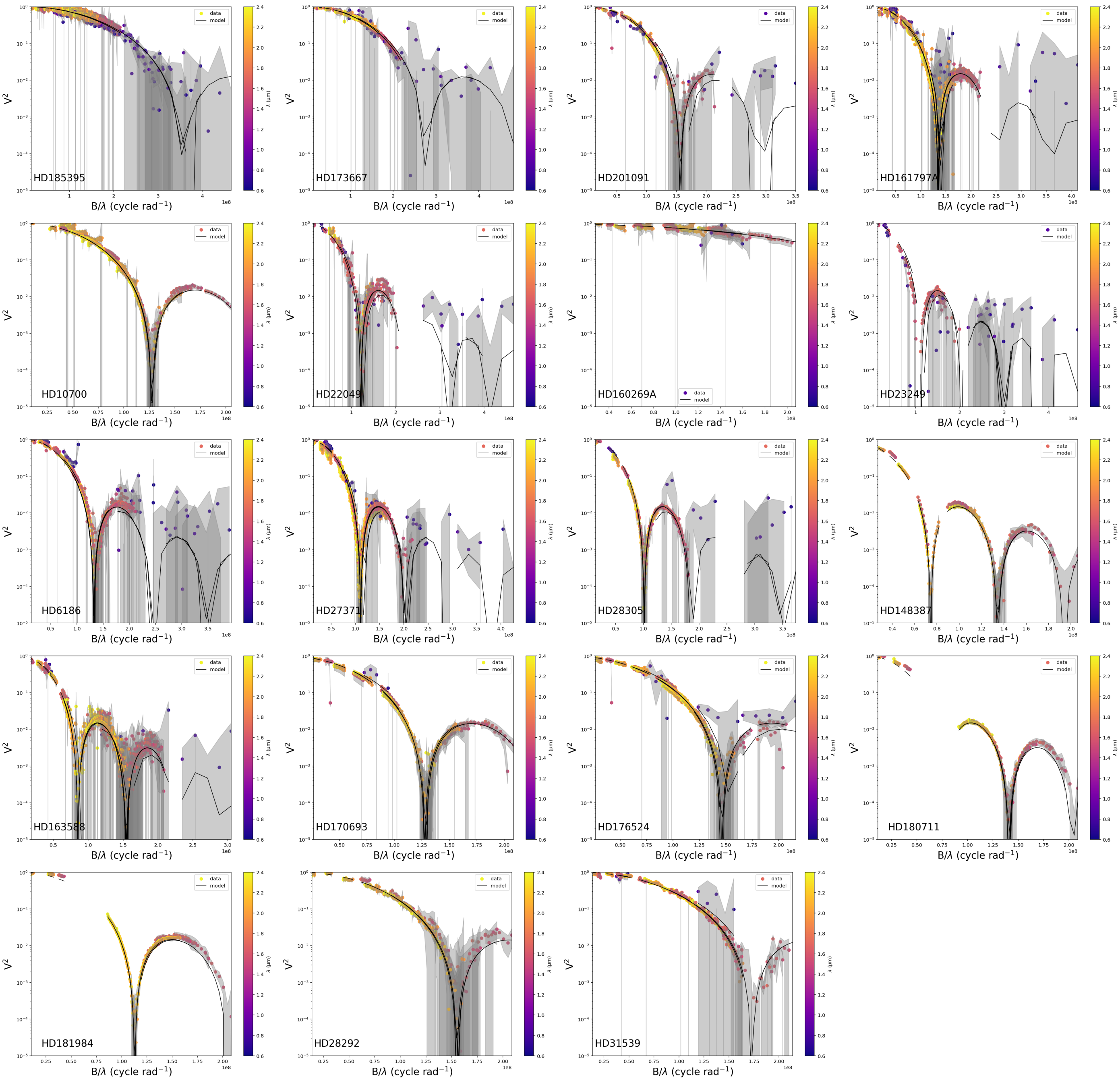

Fig. A.1: Squared visibility (in log scale) as a function of spatial frequency for the observed stars of the study. From top to bottom and left to right we have, respectively, HD185395, HD173667, HD201091, HD161797A, HD10700, HD22049, HD160269A, HD23249, HD6186, HD27371, HD28305, HD148387, HD163588, HD170693, HD176524, HD180711, HD181984, HD28292, HD31539. The dots color code indicates the wavelength of the different spectral channels. For the stars with MIRC-X, MYSTIC and SPICA data it appears as yellow for MYSTIC, red for MIRC-X and blue for SPICA. The gray zones correspond to the 1σ uncertainties on the observed data. The black line corresponds to the square root LD fit with the c and d coefficients fixed to the Claret's values.

Table B.1: Monochromatic fits for each observations in R (θ_R), H (θ_H) and K (θ_K) bands.

Star	Instrument	Date (yyyy.mm.dd)	θ_R (mas)	θ_H (mas)	θ_K (mas)
HD 173667	S	2023-08-09	0.989 ± 0.116	-	-
	SMM	2024-06-12	0.972 ± 0.176	0.959 ± 0.017	0.940 ± 0.022
	SMM	2025-04-23	1.035 ± 0.136	0.988 ± 0.063	0.949 ± 0.044
	SMM	2025-05-09	1.053 ± 0.015	0.971 ± 0.050	0.972 ± 0.047
HD 185395	S	2023-08-07	0.791 ± 0.060	-	-
	MM	2024-05-10	-	0.751 ± 0.048	0.687 ± 0.079
	SMM	2024-06-10	0.743 ± 0.018	0.734 ± 0.019	0.742 ± 0.022
	SMM	2024-06-11	0.758 ± 0.034	0.758 ± 0.028	0.785 ± 0.033
	SMM	2024-08-19	0.943 ± 0.464	0.773 ± 0.024	0.731 ± 0.072
	SMM	2025-06-14	0.753 ± 0.020	0.782 ± 0.122	0.763 ± 0.058
HD 161797A	SMM	2024-07-04	1.787 ± 0.125	1.917 ± 0.029	1.918 ± 0.010
	SMM	2025-04-23	2.262 ± 0.147	1.946 ± 0.018	1.922 ± 0.006
	SMM	2025-06-13	2.390 ± 0.484	1.923 ± 0.043	1.941 ± 0.014
	SMM	2025-08-18	1.909 ± 0.289	1.910 ± 0.064	1.928 ± 0.004
HD 10700	MM	2024-08-18	-	2.003 ± 0.152	2.021 ± 0.017
	S*MM	2024-09-14	-	2.063 ± 0.240	2.031 ± 0.150
HD 22049	S*MM	2024-09-13	-	2.118 ± 0.067	2.154 ± 0.102
	S&MIRC-X	2025-09-15	2.061 ± 0.108	2.144 ± 0.026	-
HD 160269A	SMM	2025-05-10	0.878 ± 0.058	0.670 ± 0.124	0.625 ± 0.202
HD 201091	SMM	2025-06-14	1.798 ± 0.175	1.688 ± 0.159	1.697 ± 0.042
HD 23249	S&MIRC-X	2025-09-15	2.465 ± 0.062	2.412 ± 0.090	-
HD 28305	SMM	2023-10-14	2.397 ± 0.157	2.562 ± 0.013	2.562 ± 0.011
HD 6186	S	2023-09-25	1.660 ± 0.114	-	-
	SMM	2024-08-16	1.781 ± 0.442	1.896 ± 0.248	1.887 ± 0.194
	S*&MIRC-X	2024-11-02	-	1.916 ± 0.041	-
	S*&MIRC-X	2025-08-17	-	1.921 ± 0.094	-
HD 27371	S&MYSTIC	2023-09-26	2.408 ± 0.035	-	2.374 ± 0.185
	SMM	2023-10-14	2.330 ± 0.475	2.373 ± 0.031	2.370 ± 0.097
	SMM	2023-11-10	2.092 ± 0.194	2.356 ± 0.021	2.388 ± 0.008
HD 148387	MM	2024-05-17	-	3.464 ± 0.010	3.496 ± 0.237
HD 163588	MM	2024-05-17	-	2.996 ± 0.454	3.042 ± 0.253
	S*MM	2025-05-11	-	3.015 ± 0.069	3.037 ± 0.053
	S*M*M*	2025-05-12	-	-	-
	S&MIRC-X	2025-06-14	2.942 ± 0.047	3.062 ± 0.017	-
HD 170693	MM	2024-05-19	-	2.018 ± 0.184	2.032 ± 0.025
	SMM	2025-06-15	2.108 ± 0.220	2.024 ± 0.031	2.042 ± 0.171
HD 176524	SMM	2024-07-07	1.749 ± 0.088	1.749 ± 0.110	1.775 ± 0.016
	SMM	2025-06-15	1.926 ± 0.158	1.748 ± 0.044	1.816 ± 0.004
HD 180711	MM	2024-08-17	-	3.331 ± 0.008	3.335 ± 0.025
HD 181984	MM	2024-08-17	-	2.301 ± 0.205	2.302 ± 0.011
HD 28292	MM	2024-09-12	-	1.663 ± 0.040	1.681 ± 0.022
HD 31539	SMM	2025-09-14	1.385 ± 0.173	1.513 ± 0.024	1.518 ± 0.006

Notes. S: SPICA instrument; MM: MIRC-X and MYSTIC instruments.
* Observation was considered as being not exploitable